



ELSEVIER

Nuclear Instruments and Methods in Physics Research B 194 (2002) 217–225

NIM B
Beam Interactions
with Materials & Atoms

www.elsevier.com/locate/nimb

An apparatus to measure stopping powers for low-energy antiprotons and protons

H.H. Andersen ^a, A. Csete ^b, T. Ichioka ^b, H. Knudsen ^b, S.P. Møller ^{c,*},
U.I. Uggerhøj ^b

^a Ørsted Laboratory, Niels Bohr Institute, Universitetsparken 5, DK-2100 Copenhagen Ø, Denmark

^b Institute of Physics and Astronomy, University of Aarhus, DK-8000 Aarhus C, Denmark

^c Institute for Storage Ring Facilities, University of Aarhus, Ny Munkegade, Bygn. 520, DK-8000 Aarhus C, Denmark

Received 1 November 2001; received in revised form 21 January 2002

Abstract

One of the experiments to be performed under the ASACUSA collaboration at the CERN Antiproton Decelerator is a measurement of the energy loss of low energy antiprotons in thin foils. An electrostatic spectrometer has been developed for this task. We describe the design and initial tests of the apparatus with protons. By changing a high-voltage applied on the target the energy of the projectile ions at impact on the target can easily be varied. In this way we have measured the stopping-power and the energy-loss straggling for protons over a wide energy range to below one keV. © 2002 Elsevier Science B.V. All rights reserved.

PACS: 29.30.Aj; 34.50.Bw; 61.85.+p

Keywords: Electronic stopping; Energy loss; Energy straggling; Spectrometer; Stopping power

1. Introduction

An extensive study of the energy loss of antiprotons was performed at the Low Energy Antiproton Ring, LEAR, by the PS194 collaboration. Many different solids with atomic numbers ranging from $Z_2 = 13$ to $Z_2 = 79$ were subject to investigations with antiprotons in the energy range 30 keV–3 MeV; we refer to the most recent publication [1], where references to earlier measure-

ments can also be found. As an example, in Fig. 1 are shown the measurements of antiproton stopping powers of silicon. For comparison, reference proton stopping powers are also shown [2]. The main objective of these antiproton experiments was to determine the Barkas effect in the slowing-down process, i.e. the difference in stopping power, $-dE/dx$, between positively and negatively charged particles.

New methods to measure stopping powers had to be worked out for these experiments, since the traditional methods used for protons and ions were not suited to the properties of the antiproton beam obtained at LEAR. This beam had an energy of 5.9 MeV, and an intensity of a few 100,000

* Corresponding author. Tel.: +45-8942-3778; fax: +45-8612-0740.

E-mail address: fyssp@ifau.au.dk (S.P. Møller).

per second with an emittance of around 5π mm mrad. Energies lower than the primary 5.9 MeV were obtained by slowing-down in passive degrader foils. Below around 1 MeV, the energy spread of the degraded beam was so large that the energy of the individual degraded antiprotons had to be determined. The two methods developed were based on measurements of deposited energies in silicon targets [3] and Time-Of-Flight, TOF, using secondary electrons emitted from the target foil [1].

The motivation for a continuation of these antiproton measurements is to follow the stopping power significantly below the stopping-power maximum, where the Barkas effect is no longer a perturbation to the Bethe formula applicable above the stopping-power maximum. In the LEAR measurements it was only possible for two elements, silicon and aluminium, to perform measurements at energies around a factor of two below the stopping-power maximum, see Fig. 1. In this region an *electron-gas* model of the stopping process is expected to give a good description of the slowing-down process for free-electron like materials. This model results in a velocity-proportional stopping power. Hence it is, at least at first sight, surprising that a departure from velocity-proportional stopping has only been observed for Helium [4]. Even for large band-gap insulators, deviations from velocity-proportional stopping have not been observed [5]. This has been explained by electron-

promotion processes, where electrons are promoted to molecular-like orbitals [5]. However, for antiprotons, such projectile charge-changing processes are excluded, and it should be possible to identify to what extent the binding of the target electrons influences the velocity dependence of the stopping power. In this respect, antiprotons are simpler projectiles than protons. Hence, the motivation for antiproton stopping measurements is not only to learn about the slowing down of antiprotons, but also to learn about the fundamental aspects of stopping phenomena relevant to all kinds of particles. Very recently, the newly developed *binary theory* by Sigmund and Schinner [6] has been applied to antiprotons, and here no qualitative difference is found in the stopping of metals and insulators.

In the following we will describe the apparatus designed to perform the new low-energy antiproton stopping power measurements. This experimental equipment is based on electrostatic spherical analysers. Furthermore measurements with protons will be presented. Firstly because it demonstrates the performance of the instrument, and secondly because it provides proton stopping powers and straggling at very low energies. Theoretical aspects and considerations will be included only as far as needed in the discussion.

2. Beam properties at the antiproton decelerator

Shortly after the shutdown of LEAR, it was decided to build a new antiproton facility, the Antiproton Decelerator, AD [7]. The advantage of the AD compared to LEAR is the low investment cost, as it is an updated version of the previous Antiproton Collector, and the low running costs. There are, however, also a number of disadvantages. Slow extraction giving a DC-like beam is not performed at the AD. Instead, a fast extraction delivers around 10^7 antiprotons at a kinetic energy of 5.3 MeV in a pulse of 400 ns duration once every two minutes. This beam has an emittance of 1π and 2π mm mrad for the horizontal and vertical planes, respectively. Further deceleration is needed to bring the beam below the few tens of keV appropriate for atomic physics experiments. For this

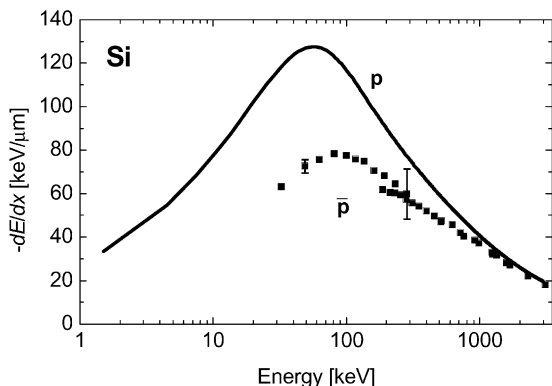


Fig. 1. Measurements of antiproton stopping powers for silicon obtained at LEAR [1]. The full-drawn curve is the recommended value for protons from [2].

purpose, the two other experiments at the AD, ATHENA and ATRAP, which aim to produce and detect antihydrogen, use degrader foils. However, the simplicity of this method is at the expense of a large loss in intensity and beam quality. For the ASACUSA collaboration, a decelerating Radio Frequency Quadrupole Decelerator (RFQD) has been built by CERN. The output energy of this device can be varied between 0 and 120 keV and the decelerating efficiency approaches 40%. For details, we refer to [8].

3. Apparatus

The somewhat remarkable beam properties at the AD-RFQD, in particular the relatively short beam pulse of very large energy spread with a low repetition rate, meant that TOF techniques were unsuited. Instead we chose to develop a spectrometer based on electrostatic spherical analysers, ESA (for a discussion of the properties of electrostatic analysers, see e.g. [9]). Due to the rather large energy spread of the beam from the RFQD, we had to build two spectrometers: one at the output of the RFQD before the target to define the incident energy and one after the target to measure the exit energy. The stigmatic focusing of spherical deflection plates means that we can obtain a small beam in both transverse directions at the position of the target and at the detector position.

Electrostatic, and magnetic, analysers have previously been used extensively for stopping power measurements. We will not here give an overview of the many experimental techniques used for measurements of proton stopping powers, mainly because the present apparatus has been tailored to the properties of the available anti-proton beam. As will be shown, the apparatus can also be used for proton beams. We refer to the discussion in [2] and references therein for a presentation and discussion of the very large number of techniques available for stopping power measurements. An exceptional feature added to the use of electrostatic energy analysers in the present work has been to change the beam energy by varying a high voltage applied to the target foil. Both acceleration and deceleration can obviously

be made. This, almost trivial, idea makes it very easy to change the beam energy without any adjustments of the accelerator, and measurements over a wide energy range become feasible with the same apparatus. An additional advantage of this technique is that even for a low-energy measurement, the beam can be transported through the analysers at high energy, where the beam emittance is low, resulting in a high transmission. Hence accurate stopping-power measurements can be made at low energy. The only disadvantage of this technique is that the relative energy change of the beam is reduced. This is, however, not a severe limitation in the present set-up with its large energy dispersion. To our knowledge, this special technique has not been widely used, although in the present investigations it has resulted in measurements of proton-stopping powers at very low energies. Below the choice of parameters for the analysers will be outlined.

In order to be able to select particles of different energy and momentum, it is necessary to have a large dispersion and a focal point at the position of the target. The dispersion for a spherical ESA is given as $D = 2R(1 - \cos(\varphi))$, where $\Delta r = D\Delta p/p$ is the deviation from the equilibrium orbit at the output where the particle has been deflected through an angle φ . The radius of curvature is R and $\Delta p/p$ is the momentum spread. We require $\Delta p/p = 0.05$ (the intrinsic spread of the RFQD beam is $\Delta T \approx 9$ keV) and a minimum resolution of $\Delta r > 10$ mm. To get a large dispersion we choose $\varphi = 90^\circ$, which gives $\Delta r = R \cdot \Delta p/p$, and finally we obtain $R > 100$ mm.

The electrical field in a spherical analyser is $E(r) = E_0(r/R)^{-2} \cong E_0(1 - 2x/R)$ where the last approximation is for a gap d much smaller than R and $r = x + R$. To second order in d/R this leads to the field $E_0V/d(1 - d^2/4R^2) \cong (V_1 - V_2)/(r_1 - r_2)$, where V_i are the electrode potentials, r_i the radii of the analyser electrodes and d is the gap distance. The required potential difference for a given kinetic energy ε is $\Delta V/d = \varepsilon/eR$. This field strength is limited due to the risk of sparks by $E_{\max} = \Delta V/d_{\max} < 1$ kV/mm and since $\varepsilon < \varepsilon_{\max} = 100$ keV we get a minimum radius of curvature $R > R_0 = \varepsilon_{\max}/(eE_{\max}) = 200$ mm. A radius of $R = 250$ mm was chosen, since this coincides with a standard

curved beam vacuum tube. Simulations show that the maximum beam radius (2σ , 95% of all particles) in the ESA is of the order 9 mm which means that half the gap distance must exceed this with some safety margin to account for a mis-steered beam etc. (still, 68% is contained within 4.5 mm). Therefore we chose $d = 20$ mm and get $\Delta V_{\max} = dE_{\max} = \varepsilon_{\max}d/eR$ corresponding to a maximum of 8 kV on each electrode.

The gap distance is also limited by $d \ll L$ and $d \ll h$, $L = R\varphi$ is the length of the electrodes and where h is the height of the electrodes to avoid significant edge focusing effects. Thus the choice of d sets a limit on h to be at least 50 mm. At the same time, the electrodes should fit into a standard beam tube with an inner diameter of 150 mm with a spacing of at least 20 mm to each side. With these restrictions, we chose h to be 60 mm to make room for the mounting and screening plates to make the field as homogeneous as possible between the ESAs.

The final issue concerns the length of the drift space between the two ESAs L_b , since this determines the initial and final drift lengths from $L_a = L_c = 2R^2/L_b$ (with $\varphi = 90^\circ$) which ensures a focus at the centre. To get a fairly small beam size through the ESAs we chose $L_a = L_c = 250$ mm and $L_b = 500$ mm. Parallel plate deflectors and Einzel lenses are installed at the entrance to the first ESA and again between the two ESAs for focusing and steering. A sketch of the apparatus with the two 90° spherical analysers is shown in Fig. 2.

The residual gas pressure inside the vacuum vessels is kept very low (around 10^{-8} mbar) in order to reduce the gas load on the RFQ system. This means that charge exchange processes due to rest-gas collisions can be completely neglected. In a transmission set-up like the present, only projectiles, which do not change charge state, are selected. This has obviously no consequences for antiprotons, but incident protons, H^+ , will during foil traversal change charge state between the three different charge states H^+ , H and H^- , and the energy loss of the projectile will depend on its charge state. For example, protons frozen in the charge state $+1$ have a significantly larger energy loss than charge states 0 and -1 , see e.g. [6]. This means that measured proton-stopping powers, for

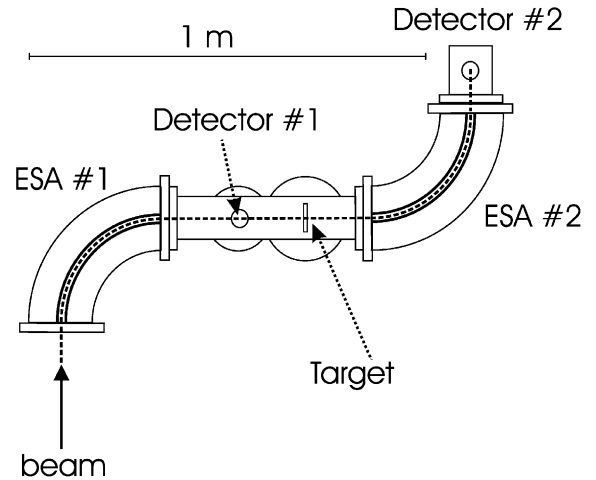


Fig. 2. Mechanical layout showing the apparatus with the two spherical analysers, target holder and channel-plate detectors.

exit charge state $+1$, will be slightly larger than the average stopping power for all incident protons. However, since the cross-sections for charge exchange are of atomic dimensions at the present projectile energies, there is a frequent shift of the projectile charge while it traverses the foil. Therefore, the measured stopping power of exiting H^+ will not differ much from the mean stopping power of all projectiles.

4. Foils and detectors

Self-supporting foils were mounted on stainless steel discs with a central hole of 10 mm. For the thinnest foils, a tungsten or nickel mesh with a large transmission was used to support the foils. Other materials, like LiF, were deposited on carbon foils. The thickness of the foils used was measured with Rutherford Back Scattering. For light foils like carbon, however, this is not possible, and the foil thickness was obtained from measurements of the stopping power for protons and comparisons to the recommended values in [2]. For carbon, aluminium, nickel and gold, we have used densities of 2.26, 2.7, 8.9 and 19.3 g/cm³, respectively, for conversion to physical thickness. The transmission of charged particles along crystalline directions in crystals, *channeling*, leads to a

reduced energy loss for positive particles. This might lead to a slight underestimate of the actual stopping cross-section by the measurements on foils, which are not amorphous. Andersen et al. [10] investigated the influence of texture in polycrystalline foils on backscattering of 2 MeV He, where the critical angle is approximately a factor of five smaller than here. For foils deposited at room temperature on amorphous backings, the dip was only 2% with a FWHM of 8° on Au and negligible for other targets used here. As the channeling influence on energy loss is less than on backscattering, and as the proton channeling dips are also more narrow here than the texture distributions, we may safely neglect the influence of channeling on the present measurements. This will to an even better approximation be the case for antiprotons [1].

The requirements to the detection system are also somewhat atypical due to the special beam properties. In particular, a position-sensitive detector with multi-particle capabilities and good intensity linearity was required. In addition, detection of both protons and antiprotons should be possible. The choice made were two-stage channel-plate detectors with optical readout by a CCD camera from a phosphor screen. In Fig. 3 are shown typical pictures from a proton beam and an antiproton beam. Isolated spots from the protons are clearly resolved, and the relative intensity can easily be determined from integrating the light on a single frame. For the antiproton beam, the situation is more complicated since all antiprotons hitting the detector will annihilate. The observed

secondary annihilation products are mainly weakly ionising high-velocity pions and recoiling, heavily ionising nuclear fragments (mainly α -particles) travelling in the plane of the detector. Examples of tracks from both of these types of particles can be seen in Fig. 3. The emitted light is still on the average proportional to the antiproton beam intensity. The fluctuations are, however, significant for small numbers of antiprotons due to the statistical nature of the annihilation process. Two detectors are installed in the apparatus: one retractable in front of the target for tuning of the first ESA to the incident beam, and one at the focal point of the second ESA for detection of the exit beam.

The measurement procedure consists then of first selecting the required incident energy by means of the first ESA. This energy has initially been calibrated against a known high voltage supply used for acceleration of the proton beam. Next, the second ESA is calibrated by transmitting this beam through the second ESA without any target foils mounted. Inserting a target foil, the exit energy can then be determined by finding the voltage of the second ESA giving maximum transmission. In practice, a scan is made of the transmitted intensity as function of the voltage of the second ESA. This distribution is then fitted with a Gaussian, and in this way the average energy can be established. The stopping power is finally deduced as $-dE/dx = (E_i - E_e)/\Delta x$ at the average energy $(E_i + E_e)/2$, where E_i and E_e are the incident and exit energies, respectively, and Δx the target thickness. Also the width, the straggling, can be extracted from this distribution. A small

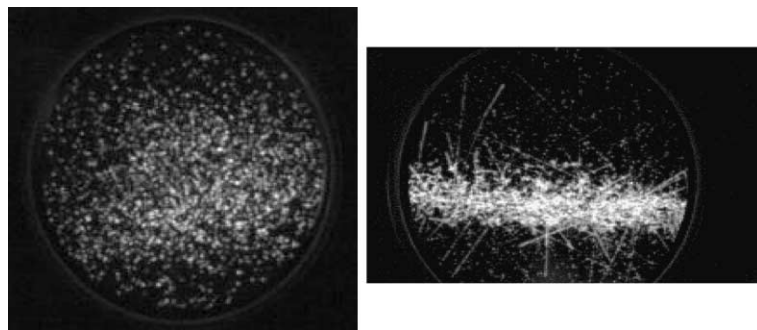


Fig. 3. Pictures of the phosphor screen of the channel-plate detector. The left picture is for a low-intensity proton beam. The picture at the right is for an antiproton beam.

error is introduced by use of the arithmetic mean for the average energy at which the stopping power is plotted, since $-dE/dx$ varies with energy. A simple estimate shows, however, that retaining the energy $(E_i + E_c)/2$ the introduced error is less than 1.5% on dE/dx even at a relative energy loss of 50%. This is a negligible error in the present investigations.

5. Proton stopping-power results

The stopping power is made up of energy transfers from so-called *electronic collisions*, where the target atoms are excited or ionised, and the *nuclear collisions*, where the energy transfer results in recoiling target atoms. The nuclear stopping only has appreciable contributions at energies of a few keV and below. For not too light targets, the nuclear stopping is around 10% at 1 keV and a few percent at 10 keV. Hence the nuclear stopping is only a small contribution, but it is naturally included in the measurements and the curves used for comparisons.

A characteristic feature of the stopping power as a function of energy is a maximum at a projectile velocity corresponding to the velocity of the target electrons, see Fig. 1. Above this maximum, the quantum-mechanical Bethe–Bloch formula including corrections gives a good quantitative description of the stopping power for particles of low charge. Below the stopping-power maximum, the classical Bohr theory applies, but quantitative results are not directly obtainable from this model. Another approach has been electron-gas calculations, but proton-stopping powers are not reproduced by such theory, presumably due to neglect of electron-capture processes.

Since the first such measurements were performed almost a century ago, a substantial amount of proton stopping power data has been accumulated. It spans a wide range of energies around the stopping power maximum for a large variety of target materials. The International Commission on Radiation Units and Measurements has published the most recent compilations, providing tabulations and fits to experimental data [2]. This reference also includes a short presentation of

experimental methods. In most cases, the largest contribution to the uncertainty of the measured stopping powers stems from incomplete control of the target properties. Depending on the material, stopping power data from [2] are accurate to 10–20% below and around the stopping-power maximum, whereas at higher energies the accuracy is in some cases below 1%. An older reference, containing recommended stopping powers for *all* materials is the compilation by Andersen and Ziegler [11]. This compilation includes references to a very large number of measurements. We also point to the web site by Paul [12], where there are references to many recent measurements. Refs. [2,11,12] also show, that there actually are only very few measurements at low energy below the stopping-power maximum.

We have measured stopping powers with the apparatus described above in the energy range 0.4–40 keV for foils of carbon, aluminium, nickel and gold. The protons were produced in a radio-frequency ion-source, and mass-selected before entering into the ESA apparatus. The beam was first optimised into a Faraday cup with a relatively high current (many nA); next, slits were closed fully, and these slits were afterwards opened slightly in order not to have too many ions impinging on the detectors ($< 10^5/s$).

The results are presented in Figs. 4–7. The measurements are made with beam energies of 8, 15 and 20 keV, and the many additional energies,

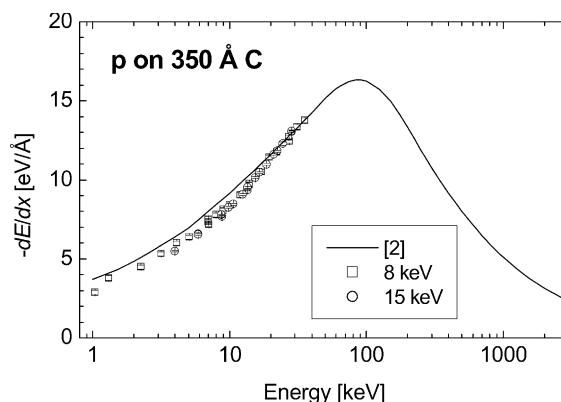


Fig. 4. Measured stopping powers of carbon for protons. The data are compared to the recommended values of [2].

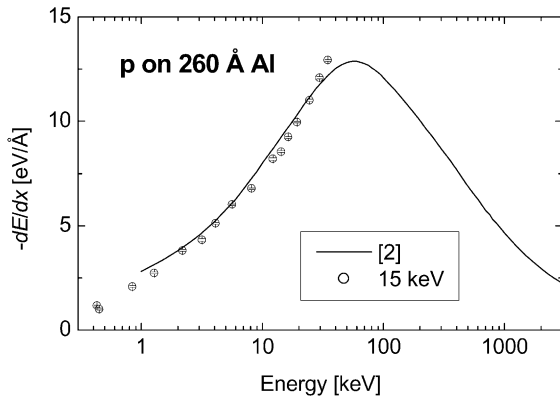


Fig. 5. As Fig. 4, but for aluminium. The data are compared to the recommended values of [2].

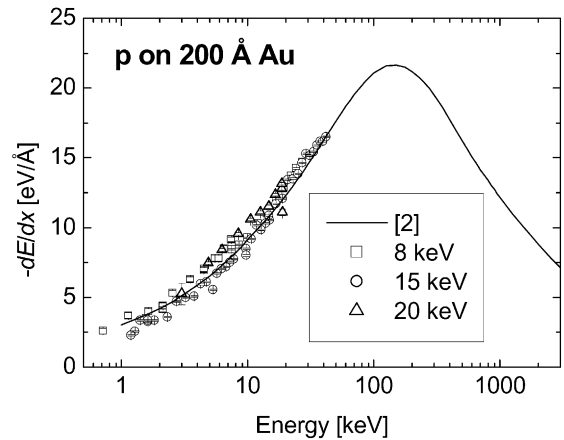


Fig. 7. Measured stopping powers of gold for protons. The data are compared to the recommended values of [2].

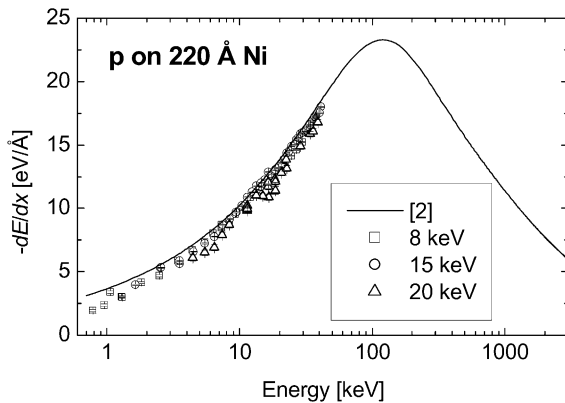


Fig. 6. Measured stopping powers of nickel for protons. The data are compared to the recommended values of [11].

at which the stopping powers were measured, were produced by biasing the target foils, as described in the previous section. The error bars correspond to thickness uncertainties of 10%. The full-drawn curves on Figs. 4–7 are the recommended stopping-powers from [2] and [11]. The measurements agree generally with the recommended curves within less than 10%, and only a few points deviate by up to 20%. In addition, we observe a good agreement between the measurements performed at the different beam energies. Furthermore, we emphasize that the measurements extend an energy range of almost two orders of magnitude, an extraordinarily wide range for a single set-up. It is,

however, also obvious that there are limitations to the method of accelerating/decelerating the projectiles upon entering the target. For example, it appears from Fig. 5, that the measured stopping powers at the very lowest and very highest energies are influenced by a systematic error. The origin of this systematic error is not identified.

In conclusion, the apparatus built has been proven to be able to measure stopping powers from energies below 1 keV to several tens of keV to an accuracy of less than 10%.

6. Energy-loss straggling results

The energy loss of a beam of particles is characterised fully by the distribution of the energy losses. This distribution is Gaussian, when the energy transfers in the individual collisions are small compared to the width of the final distribution. For low velocities as in the present experiment, this is the case for not too thin targets. The two parameters characterising this distribution are the average energy loss, determined by the stopping power described in the previous section, and the width of the distribution, the straggling. The standard deviation of the distribution is given by $\Omega^2 = N\Delta x \int T^2 d\sigma(T)$. Here N and Δx are the target atomic density and thickness, respectively, and $d\sigma$ is the cross-section differential in the energy

transfer T . For swift particles, the straggling is well approximated by the Bohr expression, $\Omega_B^2 = 4\pi Z_1^2 e^4 Z_2 N \Delta x$, obtained by insertion of the Rutherford cross-section in the previous formula. The projectile and target atomic numbers are as usual designated Z_1 and Z_2 , respectively.

When the projectile is slower than the fast, inner-shell target electrons, the straggling is reduced relative to the Bohr value, since the energy transfers in collisions with these electrons are adiabatically reduced. This effect is most easily taken into account in an electron-gas model, as was done by Lindhard and Scharff [13] and later refined by Bonderup and Hvelplund [14]. Wang and Ma [15] have obtained an analytical expression for the low-velocity asymptote. This will be used for comparisons in the present work. It should, however, be pointed out that this asymptotic expression fails around projectile energies of 50 keV, and for details above this energy, the Lindhard–Scharff or the Bonderup–Hvelplund calculations should be used. Two additional corrections to the Wang and Ma formula are, however, significant in the present region and should be included. The first is due to correlations in the electron positions in a real atomic target as opposed to an electron gas. Electrons are, both in a gas but also in a solid, concentrated around atoms and there are regions with very low electron densities. This gives rise to an additional fluctuation. We have added this atomic-correlation effect [16] to the pure electron-gas calculation by Wang and Ma. Secondly, for an inhomogeneous target with a thickness variation δx , there will be an additional straggling in the energy loss of a transmitted beam given by $\Omega^2 = (dE/dx)^2 \delta x^2$, see [16].

The measured straggling for the four different target foils used in the present proton measurements are shown in Fig. 8–11. The values have been obtained by fitting a Gaussian distribution to the measured data. The data are compared to the analytical electron-gas expression by Wang and Ma [15]. In addition, the atomic-correlation effect and a 10% inhomogeneity contribution have been added. For Ni, the calculations are shown for both 2 and 3 valence electrons. The horizontal dashed line shows the high-energy asymptote, the Bohr value. For the case of carbon, we have also in-

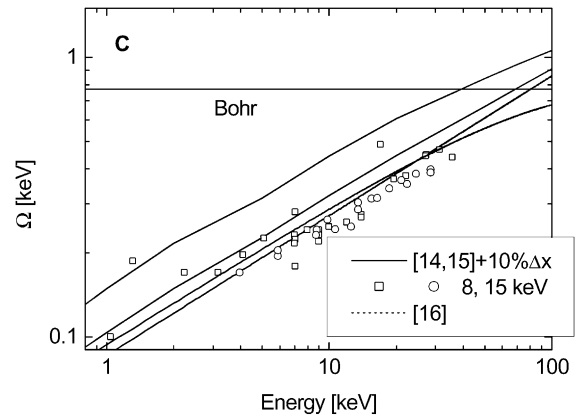


Fig. 8. Measured energy-loss straggling for protons traversing a carbon foil. The dashed curve is the Bohr value. The three full-drawn curves are from bottom the value from [15], the same including the atomic correlation effect and finally also including a 10% thickness inhomogeneity.

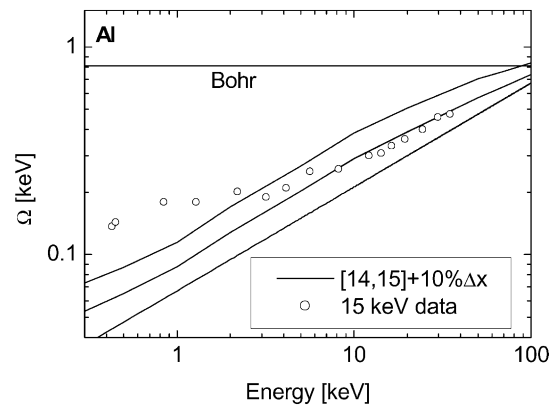


Fig. 9. The same as Fig. 8 but for aluminium.

cluded the recent data from [17] as represented by the dotted curve.

We observe that our data for all targets agree fairly well with the calculations including a small thickness variation of the order of 10%. In the case of carbon, it seems that we measure a slightly lower straggling than [17]. However, texture effects can easily influence the measurements at this level of 10%. Also for the straggling, measurements at different primary energies agree, giving confidence to the method of deceleration. In addition we observe, that at the lowest energies below a few keV,

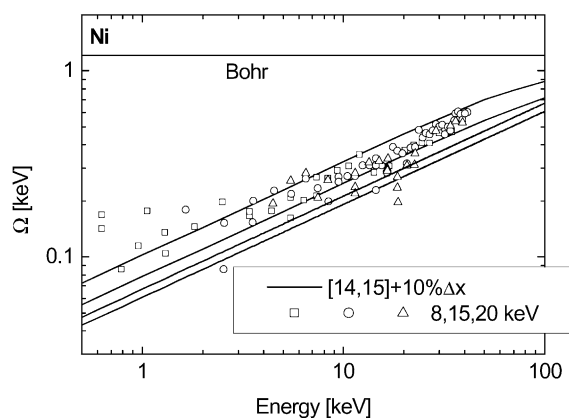


Fig. 10. The same as Fig. 8 but for nickel. The lower curve without corrections are shown for both 2 and 3 valence electrons.

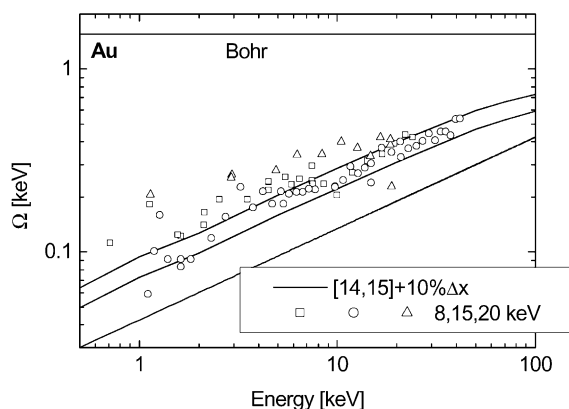


Fig. 11. The same as Fig. 8 but for gold.

the data exceed the calculated values. This could be due to the resolution of the system.

7. Summary and conclusions

We have described an apparatus based on electrostatic analysis built to measure stopping powers of solid targets for antiprotons from below 1 keV to several tens of keV. The experimental set-up has been tested with protons, and the results

confirm earlier experimental stopping powers where available. In addition, the experiment provides measurements at very small energies. Also the energy-loss straggling has been measured, and it agrees fairly well with theoretical predictions including a small thickness in-homogeneity. In conclusion, the apparatus has been proven to have the predicted and required performance, even when taking the special properties of the anti-proton beam into account. The measurements also prove the required homogeneity of the target foils.

References

- [1] S.P. Møller, E. Uggerhøj, H. Bluhme, H. Knudsen, U. Mikkelsen, K. Paludan, E. Morenzoni, *Phys. Rev. A* 56 (1997) 2930.
- [2] ICRU Report 49, Stopping Powers and Ranges for Protons and Alpha Particles, 0-913394-47-5, 1993.
- [3] S.P. Møller, *Nucl. Instr. and Meth. B* 48 (1990) 1.
- [4] R. Golser, D. Semrad, *Phys. Rev. Lett.* 66 (1991) 1831.
- [5] K. Eder, D. Semrad, P. Bauer, R. Golser, P. Maier-Komor, F. Aurmayr, M. Peñalba, A. Arnau, J.M. Ugalde, P.M. Echenique, *Phys. Rev. Lett.* 79 (1997) 4112.
- [6] P. Sigmund, A. Schinner, *Nucl. Instr. and Meth. B* 193 (2002) 49.
- [7] S. Maury, in: Proceedings from the 2001 Particle Accelerator Conference, Chicago, 18–22 June 2001.
- [8] W. Pirkel, A.M. Lombardi, Y. Bylinsky, in: Proceedings from the 2001 Particle Accelerator Conference, Chicago, 18–22 June 2001.
- [9] P. Dahl, *An Introduction to Electron and Ion Optics*, Academic Press, New York, 1973.
- [10] H.H. Andersen, K.N. Tu, J.F. Ziegler, *Nucl. Instr. and Meth.* 149 (1978) 247.
- [11] H.H. Andersen, J.F. Ziegler, *Hydrogen Stopping Powers and Ranges in all Elements*, Pergamon Press, Elmsford, New York, 1977.
- [12] Available from <http://www.exphys.uni-linz.ac.at/stopping/>.
- [13] J. Lindhard, M. Scharff, *Mat. Fys. Medd. Dan. Vid. Selsk.* 27 (15) (1953).
- [14] E. Bonderup, P. Hvelplund, *Phys. Rev. A* 4 (1971) 562.
- [15] Y.-N. Wang, T.-C. Ma, *Nucl. Instr. and Meth. B* 51 (1990) 16.
- [16] F. Besenbacher, J.U. Andersen, E. Bonderup, *Nucl. Instr. and Meth.* 168 (1980) 1.
- [17] G. Konac, S. Kalbitzer, Ch. Klatt, D. Niemann, R. Stoll, *Nucl. Instr. and Meth. B* 136–138 (1998) 159.